iScience

CellPress
OPEN ACCESS

Article

Distinct modes of telomere synthesis and extension contribute to Alternative Lengthening of Telomeres

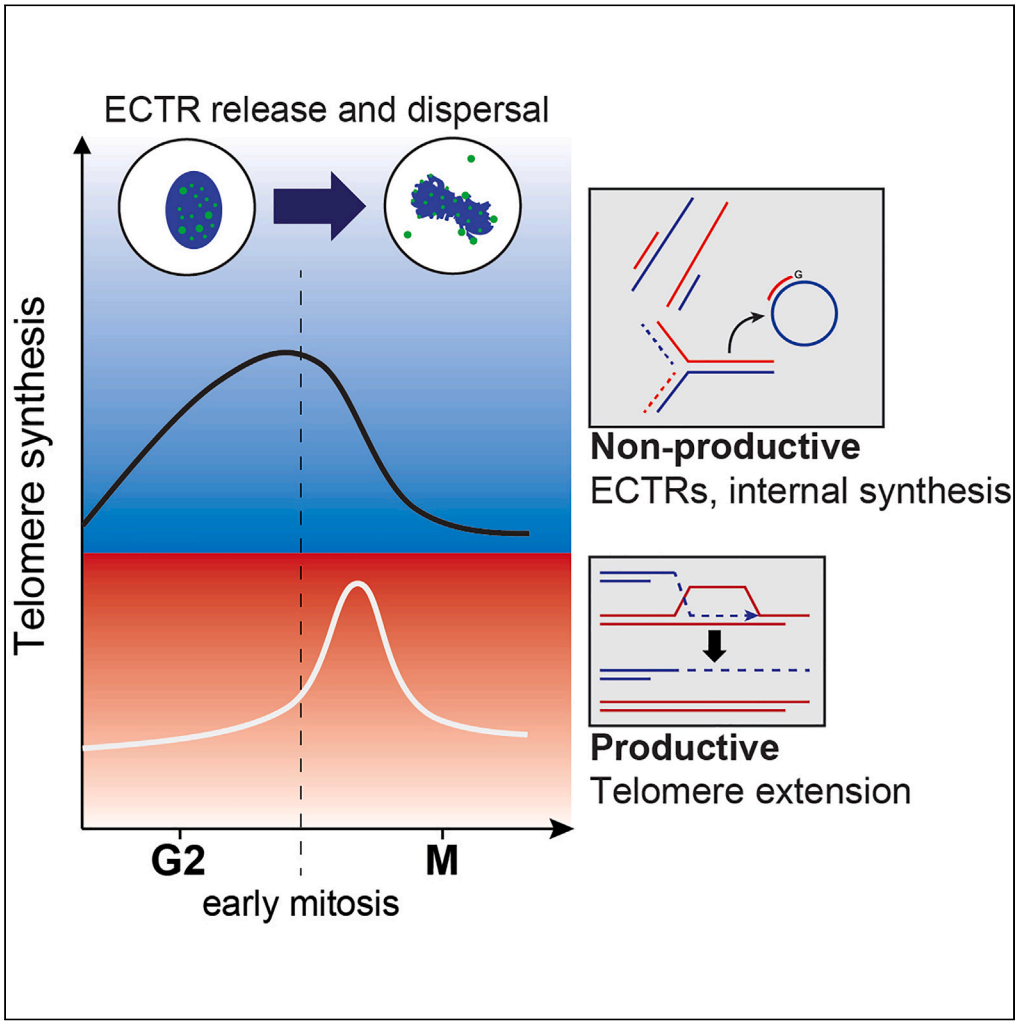

Robert Lu, Christopher B. Nelson, Samuel Rogers, Anthony J. Cesare, Alexander P. Sobinoff, Hilda A. Pickett

hpickett@cmri.org.au

Highlights

ALT cells engage in two modes of telomere synthesis

The bulk of ALT telomere synthesis takes place in G2 and is non-productive

Telomere extension predominantly occurs during the transition from G2 to mitosis

Lu et al., iScience 27, 108655
January 19, 2024
https://doi.org/10.1016/j.isci.2023.108655

iScience

CellPress
OPEN ACCESS

Article

Distinct modes of telomere synthesis and extension contribute to Alternative Lengthening of Telomeres

Robert Lu,[1] Christopher B. Nelson,[1] Samuel Rogers,[2] Anthony J. Cesare,[2] Alexander P. Sobinoff,[1] and Hilda A. Pickett[1,3,*]

SUMMARY

Alternative lengthening of telomeres (ALT) is a homology-directed repair mechanism that becomes activated in a subset of cancers to maintain telomere length. One of the defining features of ALT cells is the prevalence of extrachromosomal telomeric repeat (ECTR) DNA. Here, we identify that ALT cells engage in two modes of telomere synthesis. Non-productive telomere synthesis occurs during the G2 phase of the cell cycle and is characterized by newly synthesized internal telomeric regions that are not retained in the subsequent G1, coinciding with an induction of ECTR DNA. Productive telomere synthesis occurs specifically during the transition from G2 to mitosis and is defined as the extension of the telomere termini. While many proteins associated with break-induced telomere synthesis function in both non-productive and productive telomere synthesis, POLH specifically promotes productive telomere lengthening and suppresses non-productive telomere synthesis. These findings delineate the mechanism and cell cycle regulation of ALT-mediated telomere synthesis and extension.

INTRODUCTION

Telomeres are the nucleoprotein caps that functionally protect linear chromosome termini. Cancer cells must maintain their telomeres to proliferate indefinitely. Approximately 10–15% of cancers utilize the Alternative Lengthening of Telomeres (ALT) pathway. ALT requires a basal level of telomere damage originating from replication stress to promote unidirectional conservative telomeric DNA synthesis through the engagement of the PCNA-DNA polymerase δ break-induced replisome.[1] This pathway is consistent with a break-induced replication (BIR) or break-induced telomere synthesis (BITS) mechanism.[2]

ALT cells are characterized by heterogeneous telomere lengths, heightened telomere dysfunction, and the presence of telomere-PML colocalizations defined as ALT-associated PML bodies (APBs).[3–6] Additionally, ALT cells display prevalent extrachromosomal telomeric repeat (ECTR) species that associate with TRF1, and are constantly released from telomeres and dispersed from the nucleus.[7,8] ECTR species include double-stranded t-circles, single-stranded C-circles, and complex branched structures.[9,10] While it is unclear whether ECTRs fulfill a perpetuating role in the ALT mechanism by providing a template for telomere synthesis, or whether they are simply generated as a by-product of the pathway, their prevalence highlights substantial inefficiencies in telomere length maintenance by ALT. Furthermore, the relationship between ECTR generation and telomere extension, and the specific protein requirements, are unclear.

ALT phenotypes and ALT-mediated telomere synthesis have been observed to peak in the G2 and early M phases of the cell cycle.[5,11,12] Specifically, the ALT telomere DNA synthesis in APBs (ATSA) assay, which involves cell synchronization and EdU labeling in G2, has been used to demonstrate that ALT-specific telomere synthesis occurs exclusively in APBs.[13] Mitotic DNA synthesis (MiDAS) has also been shown to occur at ALT telomeres and is triggered by replication defects.[11] Whether G2-phase and mitotic telomere synthesis differ with respect to ECTR generation and telomere extension has been challenging to determine due to limitations in cell-based microscopy techniques, which cannot spatially resolve individual telomere synthesis events.

Here, we combine cell cycle synchronization with single molecule analysis of telomeres (SMAT) performed on stretched DNA fibers[14] to precisely measure and temporally track ALT-mediated telomere synthesis events through the cell cycle. We identify cell cycle-associated modes of non-productive and productive telomere synthesis in ALT cells. First, telomere synthesis events in G2-phase take place in APBs, but predominantly arise internally within the telomere repeat tract. These events are non-productive because they coincide with ECTR generation and a failure to retain G2-newly synthesized telomeric DNA in the subsequent cell cycle. Exacerbated G2 arrest caused by FANCM depletion[15,16] also results in the accumulation of newly synthesized telomeric DNA in APBs, which is similarly non-productive, and is dispersed into the cytoplasm during mitosis. Conversely, productive telomere extension of chromosome termini occurs during the transition from G2 phase to early mitosis. While the majority of proteins analyzed are involved in both modes of telomere synthesis, the translesion DNA

[1]Telomere Length Regulation Unit, Children's Medical Research Institute, University of Sydney, Westmead, NSW, Australia
[2]Genome Integrity Unit, Children's Medical Research Institute, University of Sydney, Westmead, NSW, Australia
[3]Lead contact
*Correspondence: hpickett@cmri.org.au
https://doi.org/10.1016/j.isci.2023.108655

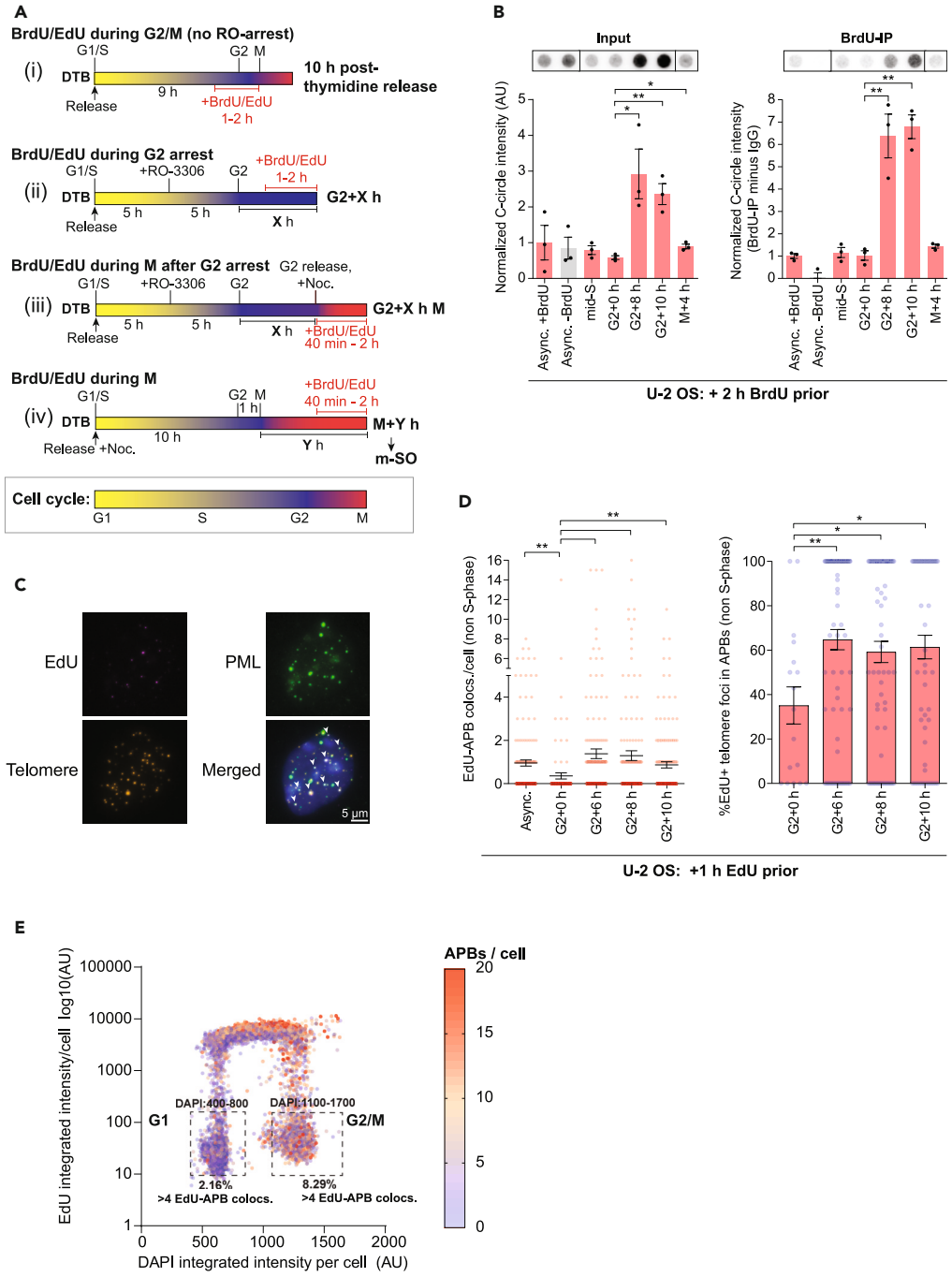

Figure 1. Non-productive telomere synthesis occurs in APBs during G2

(A) Schematic of BrdU/EdU labeling of U-2 OS cells subject to double thymidine block (DTB) then released (i) for 10 h, (ii) arrested in G2 for increasing durations with RO-3306 (G2 + X h, where X denotes the additional hours of G2 arrest), (iii) released from G2 arrest into mitosis with nocodazole (G2 + X h M, where M denotes mitotic release from G2 + X h), or (iv) synchronized directly in mitosis via the addition of nocodazole (NOC) (M + Y h, where Y denotes the additional hours of M arrest). Mitotic cells were harvested via mitotic shake-off (m-SO).

(B) Quantitation of C-circle assays on diluted genomic DNA (30 ng) and following BrdU immunoprecipitation (6 µg of input), after 2 h BrdU labeling prior to indicated asynchronous (Async.), mid-S (5 h post-thymidine release), G2 arrest (G2+0 h up to G2+10 h) or M arrest timepoints in U-2 OS cells. C-circle levels were normalized to the mean of asynchronous BrdU+ control. Error bars represent mean ± SEM out of n = 3 experiments, *p < 0.05, **p < 0.005, Student's *t* test.

(C) Representative images of telomere (orange), PML (green) and EdU (violet) colocalizations (EdU-APB colocalizations) in U-2 OS cells.

Figure 1. *Continued*

(D) Quantitation of EdU-APB colocalizations (left panel) and percentage of EdU+ telomere foci colocalizing with APBs (right panel) in U-2 OS cells after increasing the duration of G2 arrest (G2+0 h up to G2+10 h). Scatterplot bars represent the mean ± SEM. Out of three experiments, n ≥ 118 non S-phase cells were scored per treatment, **p < 0.005, Mann–Whitney test.

(E) Quantitative image-based cytometry (QIBC) plot of DAPI and EdU nuclear intensity of 10,741 asynchronous U-2 OS cells. Individual data points are color coded for number of APB colocalizations. Dashed boxes indicate the percentage of G1 or G2 gated events with >4 EdU-APB colocalizations per cell.

polymerase POLH promotes terminal telomeric MiDAS, but suppresses non-productive telomere synthesis in G2. These data characterize distinct telomere synthesis processes that contribute to the ALT pathway.

RESULTS

Newly synthesized telomeric repeat DNA accumulates during G2 phase

ALT phenotypes, including C-circles, APBs, and telomere synthesis, are elevated in G2-phase and mitosis.[11,13] To differentiate cell cycle-specific events during ALT-mediated telomere synthesis, we evaluated whether prolonged G2 or mitotic arrest led to a proportional increase in ALT phenotypes. Cells were synchronized using a double thymidine block (DTB), released, and then subjected to either (i) no G2 arrest, (ii) prolonged G2 cell-cycle arrest using RO-3306 (RO), (iii) mitotic release from RO-3306 G2 arrest, or (iv) mitotic arrest using nocodazole (Figure 1A). The cell cycle stage was confirmed via flow cytometry (Data S1A). C-circles, measured using the C-circle assay, were detected at low levels in mid-S phase (5 h post-thymidine release) and early G2 (G2+0 h), peaked after 8 h of prolonged G2 arrest (G2+8 h), and plateaued thereafter (Figure 1B).

We then measured C-circle synthesis after labeling U-2 OS cells with BrdU for 2 h in asynchronous (Async.) cells, labeling for the last 2 h of G2 arrest (G2+0 h, G2+8 h, G2+10 h) or after labeling for the last 2 h of mitotic arrest (M+4 h) (Figures 1A and 1B). C-circle amplification of BrdU immunoprecipitated DNA identified that C-circles were newly generated predominantly in the G2 phase (Figure 1B). C-circles did not accumulate in the mitotically arrested control (M+4 h) (Figure 1B), and extended mitotic arrest had no impact on C-circle levels (Data S1B).

C-circle accumulation in G2 coincided with an increase in APB frequency, telomere foci intensity in APBs, telomere synthesis in APBs, and the proportion of overall telomere synthesis occurring in APBs (Figures 1C and 1D; Data S1C). No increase in C-circles was observed following prolonged G2 arrest or in mitotically arrested telomerase-positive (ALT-negative) HeLa LT cells (Data S1D).

To further support the observation that telomere synthesis in APBs peaks in G2, we applied quantitative image-based cytometry (QIBC) to asynchronous U-2 OS cells, utilizing DAPI and EdU (labeled for 1 h) nuclear intensity to gate for G1 and G2/M populations (EdU nuclear intensity <150 AU defined as non-S-phase). After gating, we observed an increase in EdU-APB colocalizations in G2 cells compared to G1 cells (Figure 1E).[12]

Telomere synthesis events during G2 are predominantly non-terminal

To characterize the effects of cell-cycle arrest directly on telomere extension, we employed single molecule analysis of telomeres (SMAT), which utilizes molecular combing of telomere fibers.[17] Cells were labeled with EdU for 2 h (i) as cells cycled from G2 to M (10 h post-thymidine release), (ii) during G2 arrest (G2+8 h), (iii) during mitotic release from G2 arrest (G2+6 h M), or (iv) during mitotic arrest (M+4 h, M+14 h) (Figures 1A and 2B). Notably, we discovered a lack of detectable telomere extension events, defined by EdU tracts at the termini of telomere fibers, in cells labeled during G2 arrest and during mitotic arrest (Figures 2A and 2B).[18] In contrast, terminal telomere extension events were observed in cells labeled during mitotic release from G2 arrest and in control cells without RO-3306 arrest (10 h post-thymidine release) cycling from G2 to M (Figures 2A and 2B). SMAT analysis of the ALT cell line GM847 and the telomerase-positive cell line HeLa LT further demonstrated that terminal telomere extension events occur predominantly in early mitosis following release from G2, specifically in ALT cells (Figure 2C).

Detailed analysis of the SMAT tracts identified that telomere synthesis in G2 predominantly occurs non-terminally (Figures 2A and 2B), defined by the EdU tracts being generated internally within the telomere. EdU tracts originating from outside the telomere were considered to represent late replicating events and were excluded from analysis. Internal EdU tracts were maximal in G2 arrested cells, and in cycling G2/M cells without RO-3306 arrest (10 h post-thymidine release). Internal EdU tracts decreased during mitotic release from G2 and were absent in nocodazole-arrested mitotic cells (Figures 2A and 2B). These events may reflect telomere synthesis resulting from internal DNA break repair within the telomere.[2,19]

Internal telomere synthesis events are not retained at telomeres

To determine the fate of internal telomeric synthesis events generated during G2 arrest, we assessed whether they were retained in the subsequent G1 phase. U-2 OS cells were labeled with EdU for the last 1 h of G2 arrest and re-synchronized into the subsequent G1 (Figure 3A). We identified a decrease in EdU signal intensity at EdU+ telomeres in re-synchronized G1-phase cells when compared to G2-phase arrested cells (G2+0 h up to G2+10 h) (Figure 3B), indicative of a proportion of the telomere synthesis not being retained on the telomere. Cycling cells that were not subjected to an RO-3306 G2 arrest (10 h post-thymidine release) displayed minimal telomere synthesis in G2 (Figure 3B).

We rationalized that newly synthesized telomeric DNA in G2 could be lost as extrachromosomal telomeric repeats (ECTRs). To investigate this possibility, we performed cellular fractionation followed by a telomere dot-blot on DNA isolated from chromatin or cytoplasmic fractions. Purity of the fractions was verified by Western blot (Data S1E). Telomere dot-blot analysis revealed a consistent telomeric signal in the chromatin fraction across all timepoints (Figure 3C). The presence of telomeric DNA in the cytoplasmic fraction increased with prolonged G2 arrest only in the mitotically released cells (G2+0 h M, G2+6 h M, G2+10 h M), but not in the cells that remained in G2 (Figure 3C). No change in

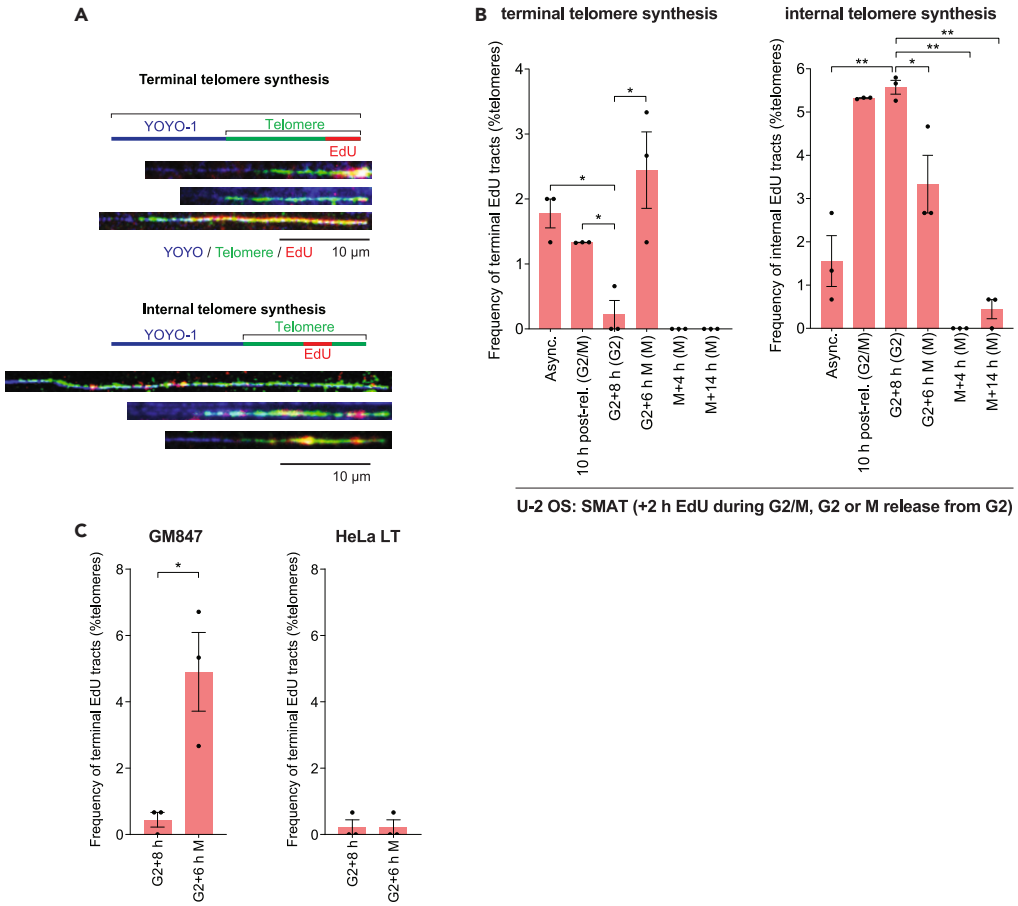

Figure 2. Telomere synthesis events in ALT cells can occur internally or terminally

(A) Definition and examples of telomere extension events (top panel) and internal EdU tracts (bottom panel) at telomere (green), EdU (red) and YOYO-1 stained (blue) DNA fibers.

(B) Quantitation of terminal telomere synthesis (left panel) and internal telomere synthesis (right panel) at indicated asynchronous, 10 h post-release, G2 arrest (G2+8 h), mitotic release from G2 (G2+6 h M) and M arrest timepoints (M+4 h, M+14 h). Error bars represent mean ± SEM of n ≥ 450 fibers out of three experiments, *p < 0.05, **p < 0.005, Student's *t* test.

(C) Quantitation of telomere extension events after 2 h EdU labeling during mitotic release in the presence of NOC (G2+6 M) in GM847 (left panel) and HeLa LT cells (right panel). Error bars represent mean ± SEM of n ≥ 450 telomeres out of three experiments, *p < 0.05, Student's *t* test.

genomic Alu repeats was observed in the chromatin fraction, and no Alu signal was detected in the cytoplasmic fraction (Figure 3C). This is indicative of the telomeric repeat DNA generated during prolonged G2 arrest being released as ECTR species upon entry into mitosis.

We then used telomere FISH combined with EdU incorporation to visualize newly synthesized telomeric DNA following mitotic release from prolonged G2. Telomere FISH was performed on cytocentrifuged mitotically enriched cells, rather than metaphase spreads, to avoid the loss of ECTRs into the supernatant (Methods S4 and S5A). An increase in the intensity of both newly synthesized chromosomal and cytoplasmic telomeric foci was observed (Figure 3D). While large telomeric foci are typically considered to comprise recombination-related clustering of individual telomeres,[20,21] we rationalized that the presence of large newly synthesized telomeric foci in the cytoplasm precludes telomere clustering, and is indicative of the loss of newly synthesized telomeric DNA into the cytoplasm as ECTRs. Live cell imaging of mCherry-TRF1-labelled telomeres identified large telomeric foci after mitotic release from G2 arrest that are dynamically associated and de-associated with chromosomes (Figures 3E–3G; Video S1). Quantitation revealed an overall gradual loss of large telomeric foci from cells following G2 arrest and mitotic release (Figure 3H), supporting telomere synthesis during G2 not being retained at the telomere. Together, the inability to retain G2-phase synthesized telomeric DNA, and the shedding of large newly synthesized telomeres during mitosis, is consistent with G2 "non-productive" telomere synthesis resulting in ECTRs.

FANCM depletion exacerbates non-productive telomere synthesis in G2

We have previously demonstrated that FANCM depletion causes a G2 arrest that coincides with rapid induction of ECTR species and telomere synthesis in APBs, in the absence of telomere lengthening.[15] This is indicative of elevated non-productive telomere synthesis. We therefore used

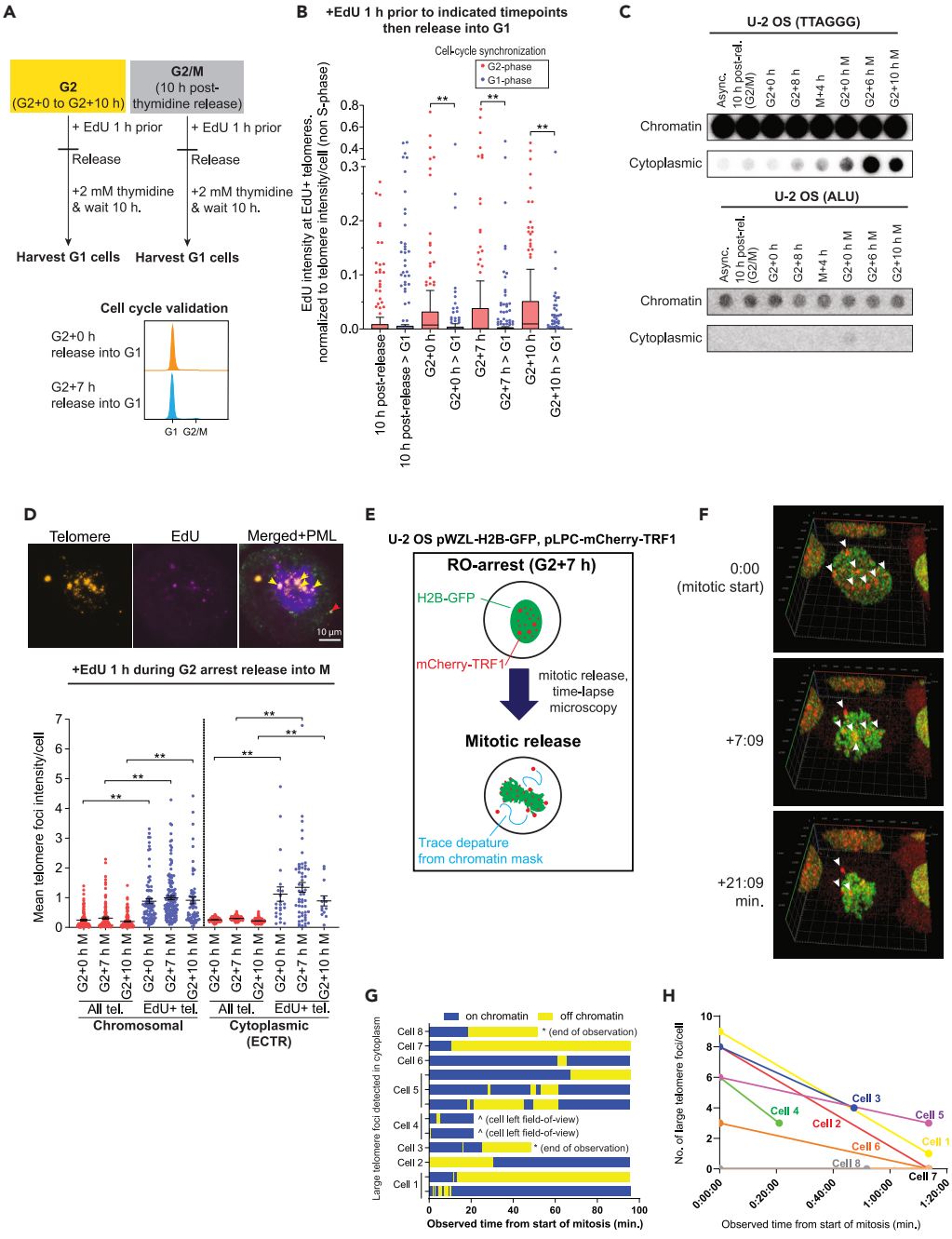

Figure 3. Telomere synthesis in G2 is not retained into the next cell cycle and coincides with ECTR generation

(A) Schematic of EdU labeling for the last hour of G2 arrest (G2+0 h up to G2+10 h) or during G2/M, from 9 to 10 h post-release (without RO-3306), followed by release into the following G1 without EdU and with thymidine for 10 h. Synchronization into the next G1 was validated by flow cytometry (bottom panel).

(B) Tukey boxplots of total EdU foci intensity at EdU+ telomeres normalized to total telomere foci intensity per non S-phase U- 2 OS cells. Cells were labeled with EdU in G2 or G2/M for 1 h, or released into subsequent G1 with thymidine for 10 h, as described in (A). Cells were labeled during G2/M (10 h post thymidine release) for 1 h as a no G2 arrest control. Out of three experiments, n ≥ 112 nuclei were scored per treatment, **p < 0.005, Mann–Whitney test.

(C) Representative denaturing dotblot for telomeres (top panel) and Alu sequence (bottom panel) from chromatin and pooled cytoplasmic DNA fractions at indicated synchronization timepoints in U-2 OS cells.

(D) Representative images (top panel) of cytoplasmic EdU+ ECTR foci (red arrow) and chromosomal EdU+ telomere foci (yellow arrow) in cytocentrifuged mitotic U-2 OS cells after EdU labeling during the last 1 h of G2 arrest (G2+7 h) followed by release into mitosis for 40 min without EdU. Quantitation of mean telomere foci intensity (bottom panel) of all telomeres and EdU+ telomeres, classified as chromosomal (overlapping DAPI mask) or cytoplasmic (not overlapping DAPI) (bottom panel – see Methods S4 for Cellprofiler scoring method and Methods S5A for synchronization schematic). Out of three experiments, n ≥ 125 mitotic cells were scored per treatment, **p < 0.005, Mann–Whitney test.

Figure 3. *Continued*

(E) Schematic of live-cell time-lapse microscopy of U-2 OS cells transduced with mCherry-TRF1 and H2B-GFP to label telomeres and chromatin respectively.
(F) Representative time-lapse images depict large telomere foci (white-arrows) either disappearing or dispersing into the cytoplasm.
(G) Timeline of large telomere foci movement classified as chromosomally attached ("on-chromatin") or in the cytoplasm ("off-chromatin") from n = 8 mitotic cells observed as described in (E). * Indicates the end of time-lapse observation. ^ Denotes when the mitotic cell disappeared from the field of view.
(H) Observed scoring of large telomere foci at the beginning of mitotic onset and at the end of the observation period (hh:min:sec) for n = 8 U-2 OS cells after mitotic release from G2 + 7 h.

FANCM siRNA depletion combined with cell synchronization to track the generation and fate of exacerbated levels of newly synthesized telomeric DNA through the cell cycle (Figures 4A and 4B). As described previously, FANCM depletion resulted in G2 arrest (Figure 4B). Using telomere FISH, PML IF, and EdU incorporation, we demonstrated that FANCM depletion induced a dramatic increase in telomere synthesis and telomere intensity in APBs during G2 (Figures 4C and 4D), while a more moderate increase in APB number was observed (Data S1F). This coincided with a dramatic induction of C-circles in FANCM depleted G2-arrested cells (Figure 4E). These data are consistent with previous reports.[15,16,22]

To determine whether the induced telomere synthesis observed following the G2 arrest caused by FANCM depletion is similarly lost in the subsequent G1, consistent with a non-productive pathway of telomere synthesis, we treated cells with the Wee1 inhibitor MK1775 to abrogate the G2/M checkpoint (Data S1G), and pulsed cells with EdU in G2 to allow for the evaluation of telomere synthesis in the subsequent G1 (Figure 4F). As FANCM depletion induces G2 cell-cycle arrest, a DMSO control was not included for the Wee1 inhibitor. By quantitating EdU intensity at EdU+ telomeres, we found that the exacerbated telomere synthesis attributed to FANCM depletion was lost in the subsequent G1 (Figure 4G), indicative of non-productive telomere synthesis. Using telomere FISH on mitotic cells (Methods S4), we identified an increase in both ECTR foci and newly synthesized ECTR foci in FANCM depleted cells compared to siRNA control following Wee1 inhibition (Figure 4H), consistent with newly synthesized telomeric DNA being generated at telomeres and then lost as ECTR species.

Terminal telomere synthesis predominates in early mitosis

Considering that ALT cancers exhibit elevated telomere MiDAS,[11,21,23] combined with our observation of terminal extension events during mitosis, we next examined the nature and fate of mitotic telomere synthesis. U-2 OS cells were labeled with EdU for 2 h during mitotic release from G2 arrest (G2+6 h M), and were then re-synchronized in the subsequent G1 with thymidine (Figure 5A). SMAT analysis identified a similar proportion of telomere extension events following mitotic release compared to that retained in the subsequent G1 (Figure 5B), indicative of telomere lengthening in early mitosis being "productive," due to its retainment at telomeres.

To further characterize conservative telomere synthesis, indicative of BIR, we measured single-chromatid EdU-positive telomeres on metaphase spreads after sequential BrdU labeling in G2 for 1 h followed by EdU labeling for 40 min during mitotic release (Figure 5C). We observed that most of the telomere synthesis events detected in metaphase had commenced in G2 (BrdU) and were either restricted to G2 (BrdU) or progressed during the transition from G2 into mitosis (BrdU/EdU) (Figure 5D). Only a small proportion of single-chromatid telomere synthesis events have been initiated exclusively in mitosis (EdU) (Figure 5D). These data suggest that the majority of telomere synthesis events detected in metaphase spreads are likely carry-over from G2-initiated synthesis.

We then performed SMAT analysis after sequential BrdU labeling for 2 h in G2 followed by EdU labeling for 2 h during mitotic release with nocodazole (Figures 5E and 5F). Consistent with our previous observations, terminal BrdU and BrdU/EdU extension events were lacking. Only EdU extension events were observed, suggesting terminal productive telomere synthesis events only occur during mitosis (Figure 5F). In contrast, internal non-productive telomere synthesis events occurred during G2 and were carried over into mitotic release (Figure 5F).

Translesion polymerase POLH promotes terminal telomere extension, but suppresses non-productive telomere synthesis

Our data indicate that telomeric DNA is synthesized in both G2 and mitosis. However, G2 synthesis is predominantly non-productive, coinciding with the generation of ECTR species and the loss of newly synthesized telomeric DNA in the following G1. To characterize these two phases of telomere synthesis, we evaluated the protein requirements of G2 and mitotic telomere synthesis. First, we used siRNA depletion to investigate BIR factors BLM, POLD3, RAD51, RAD52, and the translesion polymerase POLH (Data S2A). Cells were synchronized and labeled with EdU (Figure 6A). Depletion of PML, which is required for ALT telomere maintenance,[24] was included as a positive control (Data S2B).

A significant decrease in telomere synthesis in APBs after prolonged G2 arrest was observed following PML and BLM depletion, while a significant increase in telomere synthesis was observed with POLH depletion (Figure 6B). C-circle levels and ECTR generation also decreased with PML and BLM depletion, but increased following POLH depletion (Figures 6C and 6D). RAD51 depletion had a significant effect, increasing telomere synthesis in G2 and to a lesser extent ECTR generation compared to the scrambled control, while both RAD52 and POLD3 depletion resulted in a small reduction in telomere synthesis in APBs independent of APB and ECTR frequency (Figures 6B–6D, Data S2B). SMAT analysis of terminal telomere extension events in cells subjected to prolonged G2 arrest followed by mitotic release demonstrated a significant decrease in the frequency of terminal extension events with the depletion of all BIR factors, as well as with the depletion of PML and POLH (Figure 6E). These data suggest that, while BIR factors contribute to both G2 and mitotic telomere synthesis, the translesion DNA polymerase POLH promotes terminal mitotic telomere synthesis, but appears to inhibit internal telomere synthesis during G2.

To further characterize the process by which newly synthesized non-terminal telomeric DNA is lost upon entry into mitosis, we used siRNA depletion of the structure-specific endonucleases MUS81, SLX4, and GEN1 (Methods S5B), which have established roles in cleaving t-loop structures and stalled fork substrates, in synchronized cells labeled with EdU. A significant decrease in telomere synthesis in APBs during

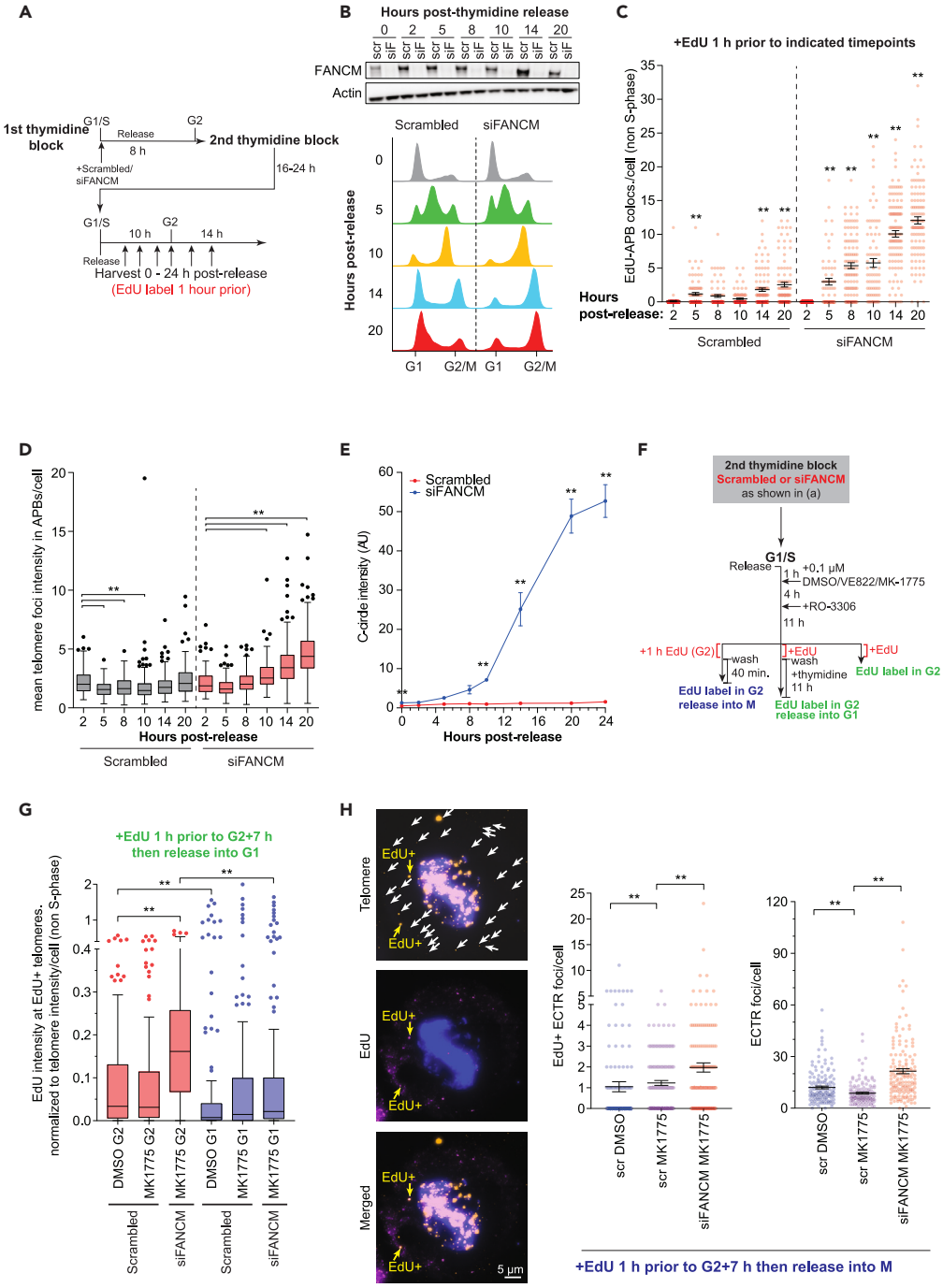

Figure 4. FANCM depletion exacerbates non-productive telomere synthesis during G2

(A) Schematic of U-2 OS cell synchronization at the G1/S boundary in coordination with siRNA depletion (Scrambled or siFANCM). siRNA treated cells were optionally labeled with EdU for 1 h prior to analysis at indicated timepoints post-thymidine release.

(B) Western blot and cell-cycle validation of FANCM depletion at indicated timepoints.

(C) Quantitation of EdU- APB colocalizations and (D) mean telomere foci intensity in APBs in non S-phase FANCM-depleted U-2 OS cells at indicated timepoints post thymidine release. Scatterplot bars represent the mean ± SEM. Out of three experiments, n ≥ 150 nuclei were analyzed per treatment. Statistics are relative to 2 h post-release Scrambled or siFANCM timepoint. **p < 0.005, Kruskal-Wallis ANOVA test.

(E) C-circle assay quantitation in U-2 OS cells depleted of FANCM at indicated timepoints from n = 3 experiments. C-circle levels were normalized to U-2 OS asynchronous reference control, **p < 0.005, Student's *t* test.

Figure 4. *Continued*

(F) Schematic of U-2 OS cell synchronization and release, addition of 0.1 μM DMSO or MK1775 with RO-3306 for synchronization in G2. Cells were labeled with EdU during the last hour of G2 arrest followed by release into G1 without EdU. Cells either in G2 or G1 were analyzed for EdU-telomere colocalizations or released into mitosis for 2 h with EdU for SMAT.

(G) Tukey boxplots of total EdU foci intensity at EdU+ telomeres normalized to total telomere foci intensity per non S-phase U-2 OS cells depleted of FANCM and treated with DMSO or MK1775. Cells were labeled with EdU in the last 1 h of G2 (red) then released in the subsequent G1 (blue) as described in (F). Out of three experiments, n = 120 non S-phase nuclei were analyzed per treatment. Statistics are relative to Scrambled DMSO G2 or Scrambled DMSO G1 treatments, **p < 0.005, Kruskal-Wallis ANOVA test.

(H) Representative images (left panel) of cytocentrifuged mitotic U-2 OS cells depleted of FANCM following treatment with DMSO or MK1775 and EdU-labelling in G2 as described in (F). Mitotically enriched cells were stained for telomeres (yellow) and EdU (violet) and quantitated for EdU+ ECTRs (yellow arrows) and ECTR foci (white arrows) per cell (right panels). See Methods S4 for Cellprofiler scoring method. Scatterplot bars represent the mean ± SEM. Out of three experiments, n ≥ 139 mitotic cells were scored per treatment, **p < 0.005, Mann–Whitney test.

prolonged G2 was observed following MUS81 depletion, while the depletion of SLX4 and GEN1 had no effect (Figure 6F). SMAT analysis demonstrated a significant decrease in the frequency of telomere extension events after MUS81 depletion. No change was observed with GEN1 depletion, while SLX4 depletion slightly increased the frequency of extension events (Figure 6G). These data are indicative of MUS81 contributing to ALT-mediated telomere synthesis.

DISCUSSION

The ALT pathway involves an amalgamation of homologous recombination pathways that functionally extend telomeres to compensate for telomere erosion by maintaining telomere length. Multiple hallmarks of ALT activity exist, including long and heterogeneous telomere lengths, ECTR species, telomere sister-chromatid exchange (T-SCE) events, telomere dysfunction-induced foci (TIF), ultrabright telomeric foci, telomeric MiDAS, the presence of APBs, and the detection of G2 telomere synthesis in APBs. There is currently no biochemical assay that directly measures ALT activity. Levels of different biomarkers can vary between cells and cell lines, reflecting a level of variability in the ALT mechanism, and making robust classification of ALT reliant on the presence of several biomarkers.[25] Importantly, many ALT biomarkers are not directly attributable to ALT-mediated telomere extension, but rather represent phenotypic characteristics either associated with the mechanism or generated as a consequence of it. This marks a stark problem when detecting ALT activity using biomarkers, without fully understanding their origin and relevance. In this study, we aimed to address this gap in our understanding by using cell synchronization and telomere fiber analysis to track telomere synthesis events in ALT cells through the cell cycle.

We demonstrate that telomere synthesis occurs predominantly in G2, consistent with previous reports. However, our data indicate that these synthesis events are internal within the telomere repeat tract. Internal telomere synthesis events dominate in ALT cells, and are non-productive. This is evident by the concomitant accumulation of newly synthesized telomeric DNA as ECTRs during prolonged RO-3306 or FANCM-depletion induced G2 arrest, and by the loss of telomeric DNA that is newly synthesized during G2 in the subsequent G1 phase of the cell cycle. Overall, our data implicate a pathway of internal telomere synthesis, followed by excision and removal from the cell (Figure 7), which seems counterintuitive to telomere length maintenance, but consistent with ALT phenotypes.

Internal telomere tract synthesis does not align with telomere extension by break-induced replication, which, once initiated, progresses to the end of the template strand; however, is consistent with the formation and prevalence of internal loops (i-loops) at ALT telomeres.[26] I-loops comprise the majority of telomeric structures detected in ALT cells and have been suggested to be structural transitions that occur at nicks and gaps that culminate in circular ECTR excision products. While it is unclear whether i-loops are newly synthesized, they do appear to represent a response to telomeric damage.

We further demonstrate that terminal telomere synthesis, consistent with break-induced replication, is detected upon mitotic release from G2. Terminal telomere synthesis events are not detected in G2 or in mitotically arrested cells. This suggests that the productive telomere synthesis that is responsible for ALT-mediated telomere extension is limited to after the G2/M transition, potentially occurring during early mitosis. Despite clear overlap of the proteins involved in both modes of telomere synthesis, including BLM, RAD52, and POLD3, we identify a distinct role for POLH in promoting terminal productive telomere synthesis during mitotic release from G2, while suppressing telomere synthesis in G2. This differential could be attributed to the requirement for increased damage tolerance in terminal break-induced telomere synthesis.

Finally, we find that prolonged G2 arrest following treatment with RO-3306 results in an artifactual increase in both telomere synthesis in APBs and C-circle levels, and that MiDAS detection on metaphase spreads cannot differentiate between internal non-productive telomere synthesis versus terminal productive telomere synthesis. This is relevant, as RO-3306-mediated G2 arrest is incorporated into both the ATSA and MiDAS assays. Furthermore, our data indicate that telomere MiDAS is likely to be contaminated by carry-over G2 synthesis. Rigorous detection of telomere MiDAS can be achieved on metaphase spreads by sequential labeling with dual thymidine analogues in G2 and following mitotic release, or by employing telomere fiber analysis.

Overall, the characterization of the cell cycle intricacies of telomere synthesis using DNA fiber analysis has identified internal non-productive and terminal productive modes of telomere synthesis in ALT cells. Non-productive telomere synthesis events dominate and coincide with the production of ECTRs, consistent with the abundance of EdU incorporated telomeric DNA in APBs during G2 and the prevalence of ECTR species in ALT cells. In contrast, productive telomere extension events are less frequent. This exposes the ALT pathway as an inefficient mechanism of telomere length maintenance, and raises questions as to why these inefficiencies exist. Potentially, the telomere lengths achieved by

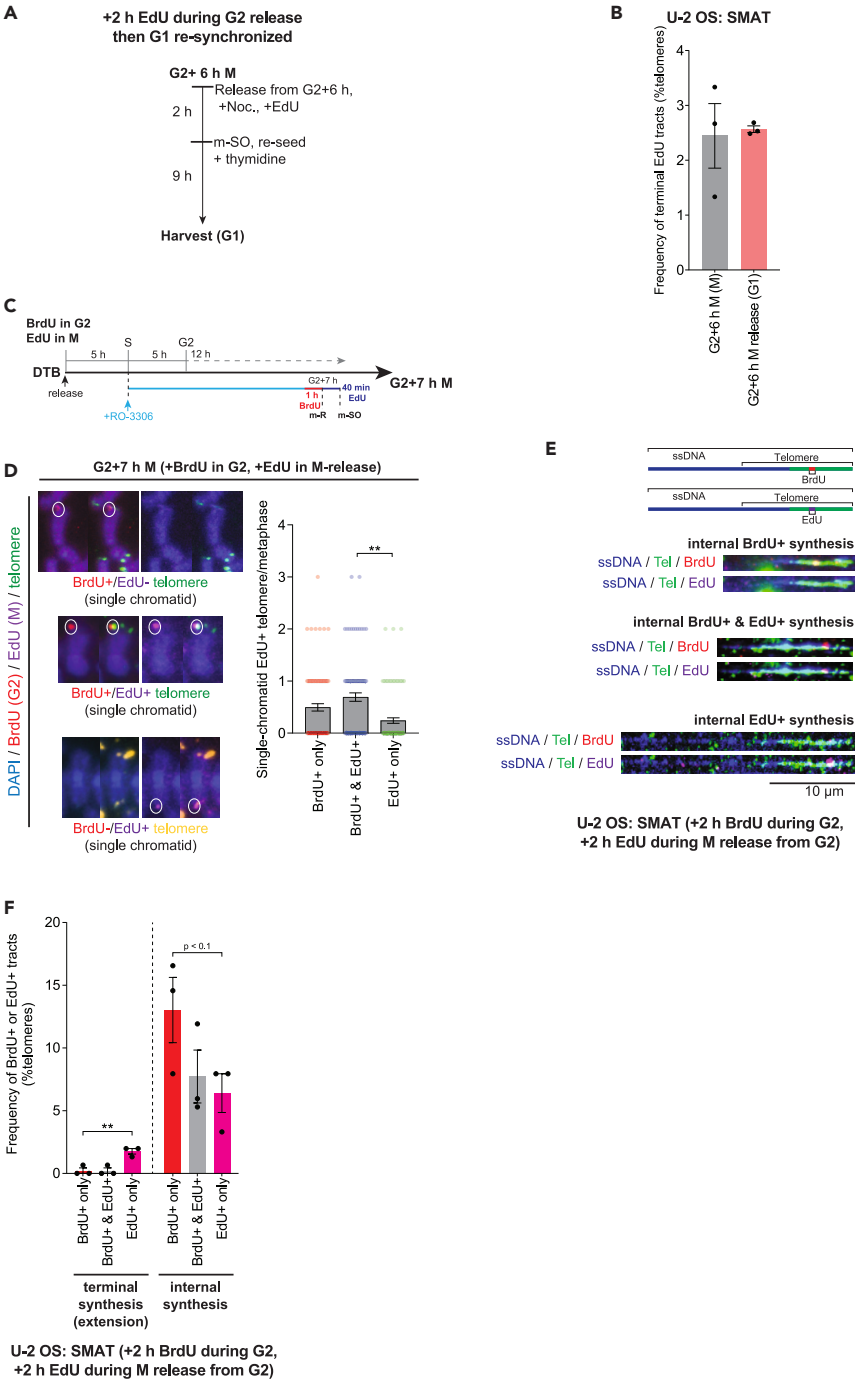

Figure 5. Terminal telomere synthesis occurs in early mitosis

(A) Schematic of SMAT EdU labeling for 2 h during mitotic release after G2 arrest with nocodazole (G2+6 h M) followed by mitotic shake-off, re-seeding without EdU in the presence of thymidine for resynchronization into the subsequent G1.

(B) Quantitation of telomere extension events in G1 resynchronized U-2 OS cells after 2 h EdU labeling during mitotic release (G2+ 6 h M) as described in (A) and Figure 2A. Frequency of telomere extension events for G2+6 h M, from the previous cell cycle (Figure 2B), are re-displayed for comparison. Error bars represent mean ± SEM of n ≥ 450 telomeres out of three experiments, *p < 0.05, Student's *t* test.

(C) Schematic of cell synchronization via DTB and G2 arrest at G2+7 h M. Cells were labeled with BrdU during the last 1 h of G2+7 h G2 arrest, washed then released into mitosis with EdU for 40 min (G2+7 h M).

(D) Representative images of telomere (green/yellow), BrdU-labelled (red), EdU-labelled (violet) single-chromatid telomere colocalizations from metaphase spreads in U-2 OS cells (left panel). Cells were labeled as described in (C) and harvested via mitotic shake-off. Quantitation of single-chromatid

Figure 5. *Continued*

colocalizations of telomeres with BrdU+ only, BrdU+ and EdU+ or EdU+ only (right panel). Scatterplot bars represent the mean ± SEM. Out of three experiments, n = 91 metaphases were scored, **p < 0.005, Mann–Whitney test.

(E) Representative SMAT images of BrdU+ only (top panel), BrdU+ and EdU+ (middle panel) and EdU+ only (bottom panel) internal synthesis events at telomere tracts (green) on DNA fibers (blue). BrdU (red) was labeled in the last 2 h of G2+8 h G2 arrest followed by EdU (violet) labeling for 2 h during G2 release into mitosis with NOC.

(F) SMAT quantitation of terminal extension and internal synthesis events at telomere tracts, classified as BrdU+ only, BrdU+ and EdU+ or EdU+ only. Error bars represent mean ± SEM of n ≥ 450 telomeres out of three experiments, *p < 0.05, **p < 0.005, Student's *t* test.

a more productive or successful ALT mechanism would be detrimental to cells, and a balance between non-productive and productive synthesis is optimal for cell proliferation and survival.

Limitations of the study

This study demonstrates the cell-cycle regulation of telomere synthesis in ALT cells. We show that most ALT-specific telomere synthesis outside of S-phase occurs in G2 and is predominantly non-productive. We rely extensively on RO-3306 to observe these events. RO-3306 is used widely in the ALT telomere biology field to assess telomere synthesis during G2-phase.[11] However, prolonged arrest with RO-3306 can alter replication dynamics and lead to defects in mitotic progression. Therefore, our results may not completely recapitulate the extent of non-productive telomere synthesis in unchallenged ALT cells. This is an issue endemic to the ALT field, and it remains a challenge to accurately observe telomere synthesis events independent of cell cycle manipulation.[27]

STAR★METHODS

Detailed methods are provided in the online version of this paper and include the following:

- KEY RESOURCES TABLE
- RESOURCE AVAILABILITY
  - Lead contact
  - Materials availability
  - Data and code availability
- EXPERIMENTAL MODEL AND SUBJECT DETAILS
  - Cell culture
- METHOD DETAILS
  - Synchronization of cell lines and BrdU/EdU labeling
  - Genetic constructs and plasmids
  - RNA interference
  - Genomic DNA extraction and purification
  - Immunoblotting
  - Single molecule analysis of telomeres (SMAT)
  - Standard C-circle assay and newly synthesized C-circle assay (native BrdU immunoprecipitation)
  - Cell fractionation for Southern blotting
  - Immunofluorescence (IF) and fluorescence in situ hybridization (FISH)
  - Dropped chromosome metaphase spread analysis
  - BrdU and EdU detection for microscopy
  - Live cell imaging
  - Cellprofiler microscopy image analysis
  - Flow cytometry
- QUANTIFICATION AND STATISTICAL ANALYSIS

SUPPLEMENTAL INFORMATION

Supplemental information can be found online at https://doi.org/10.1016/j.isci.2023.108655.

ACKNOWLEDGMENTS

The authors acknowledge the Australian Medical Research Future Fund (2007488) and the National Health and Medical Research Council of Australia (1162886) for funding.

AUTHOR CONTRIBUTIONS

R.L. performed experiments. R.L. and C.B.N. analyzed the data. H.A.P. and A.P.S. supervised the study. H.A.P., R.L. and A.P.S wrote the article. All authors have read and edited the article. S.R. and A.J.C. made and provided the U-2 OS cells, which were stably transduced with pWZL-H2B-GFP and pLPC-mCherry-TRF1.

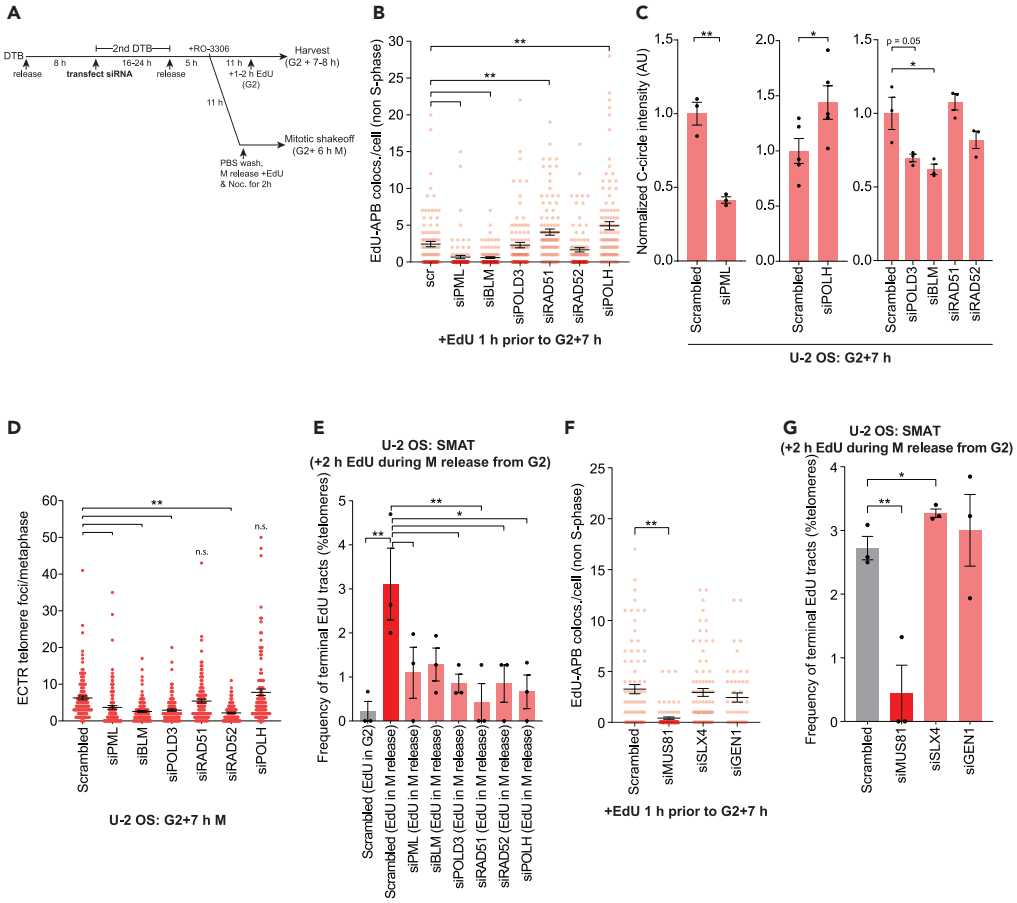

Figure 6. POLH suppresses non-productive telomere synthesis

(A) Schematic of U-2 OS cell synchronization at the G1/S boundary in combination with siRNA depletion after first DTB and prior to the second DTB then G2 arrest with RO-3306. Cells were then either harvested in G2 after 1 h EdU labeling or released into mitosis with EdU and nocodazole for 2 h for SMAT. Schematic applies to b-e.

(B) Quantitation of EdU-APB colocalizations in non S-phase U-2 OS cells for indicated siRNA depletions and arrested in G2 after 1 h EdU labeling at the end of G2+7 h. Scatterplot bars represent the mean ± SEM. Out of three experiments, n = 100 non S-phase cells were analyzed per treatment. Statistics are relative to scrambled control, **p < 0.005, Kruskal-Wallis ANOVA test.

(C) Quantitation of C-circle assay for U-2 OS cells depleted of PML (left panel), POLH (middle panel) and POLD3, BLM, RAD51, RAD52 (right panel) after G2 arrest (G2+7 h). Error bars represent mean ± SEM out of n = 3 experiments, **p < 0.005, Student's *t* test.

(D) Quantitation of ECTR foci from cytocentrifuged mitotic U-2 OS cells, for indicated siRNA treatments after EdU labeling during the last 1 h of G2 arrest (G2+7 h) followed by release into mitosis for 40 min without EdU. Scatterplot bars represent the mean ± SEM. Out of three experiments, n ≥ 115 cells were scored per treatment, **p < 0.005, Mann–Whitney test.

(E) Quantitation of telomere extension events for the indicated siRNA depletions after G2 release (G2+6 h M) into mitosis with EdU and nocodazole for 2 h according to (A). Error bars represent mean ± SEM of n ≥ 450 telomeres out of three experiments, *p < 0.05, **p < 0.005, Student's *t* test.

(F) Quantitation of EdU-APB colocalizations in U-2 OS cells depleted for MUS81, SLX4 or GEN1 and arrested in G2 after 1 h EdU labeling (G2+7 h). Scatterplot bars represent the mean ± SEM. Out of three experiments, n ≥ 46 non S-phase cells were scored per treatment, **p < 0.005, Mann–Whitney test.

(G) Quantitation of telomere extension events for indicated MUS81, SLX4 or GEN1 siRNA depletion after G2 release (G2+6 h M) into mitosis with EdU and nocodazole for 2 h. Error bars represent mean ± SEM. Out of three experiments, *p < 0.05, **p < 0.005, Student's *t* test.

For (F) and (G) siRNA transfection was performed to a modified synchronization schematic as described in Methods S5B.

DECLARATION OF INTERESTS

H.A.P. is a founder of Tesellate Bio and a member of its scientific advisory board.

Received: August 7, 2023
Revised: October 13, 2023
Accepted: December 4, 2023
Published: December 11, 2023

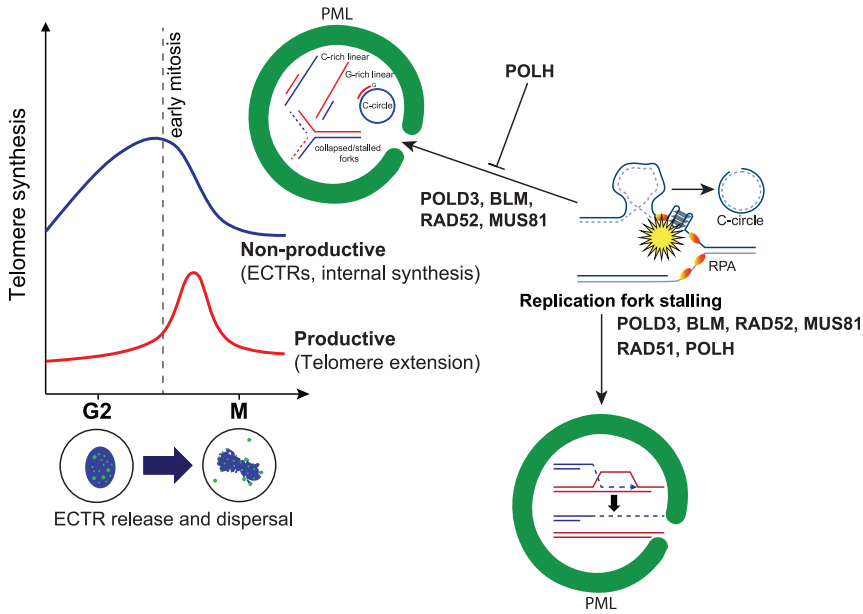

Figure 7. Summary model of telomere synthesis in ALT cells

Non-productive telomere synthesis defined by internal telomere synthesis coinciding with ECTR generation peaks in G2-phase and decreases as cells enter mitosis. While core break-induced telomere synthesis (BITS) factors BLM, POLD3 (of Pol δ), PML, and to an extent RAD52, are required for both modes of telomere synthesis, POLH promotes only mitotic productive telomere extension.

REFERENCES

1. Zhang, T., Rawal, Y., Jiang, H., Kwon, Y., Sung, P., and Greenberg, R.A. (2023). Break-induced replication orchestrates resection-dependent template switching. Nature *619*, 201–208.
2. Dilley, R.L., Verma, P., Cho, N.W., Winters, H.D., Wondisford, A.R., and Greenberg, R.A. (2016). Break-induced telomere synthesis underlies alternative telomere maintenance. Nature *539*, 54–58.
3. Cesare, A.J., Kaul, Z., Cohen, S.B., Napier, C.E., Pickett, H.A., Neumann, A.A., and Reddel, R.R. (2009). Spontaneous occurrence of telomeric DNA damage response in the absence of chromosome fusions. Nat. Struct. Mol. Biol. *16*, 1244–1251.
4. Yeager, T.R., Neumann, A.A., Englezou, A., Huschtscha, L.I., Noble, J.R., and Reddel, R.R. (1999). Telomerase-negative immortalized human cells contain a novel type of promyelocytic leukemia (PML) body. Cancer Res. *59*, 4175–4179.
5. Zhang, T., Zhang, Z., Shengzhao, G., Li, X., Liu, H., and Zhao, Y. (2019). Strand break-induced replication fork collapse leads to C-circles, C-overhangs and telomeric recombination. PLoS Genet. *15*, e1007925.
6. Bryan, T.M., Englezou, A., Dalla-Pozza, L., Dunham, M.A., and Reddel, R.R. (1997). Evidence for an alternative mechanism for maintaining telomere length in human tumors and tumor-derived cell lines. Nat. Med. *3*, 1271–1274.
7. Ogino, H., Nakabayashi, K., Suzuki, M., Takahashi, E., Fujii, M., Suzuki, T., and Ayusawa, D. (1998). Release of telomeric DNA from chromosomes in immortal human cells lacking telomerase activity. Biochem. Biophys. Res. Commun. *248*, 223–227.
8. Tokutake, Y., Matsumoto, T., Watanabe, T., Maeda, S., Tahara, H., Sakamoto, S., Niida, H., Sugimoto, M., Ide, T., and Furuichi, Y. (1998). Extra-chromosomal telomere repeat DNA in telomerase-negative immortalized cell lines. Biochem. Biophys. Res. Commun. *247*, 765–772.
9. Nabetani, A., and Ishikawa, F. (2009). Unusual telomeric DNAs in human telomerase-negative immortalized cells. Mol. Cell Biol. *29*, 703–713.
10. Henson, J.D., Cao, Y., Huschtscha, L.I., Chang, A.C., Au, A.Y.M., Pickett, H.A., and Reddel, R.R. (2009). DNA C-circles are specific and quantifiable markers of alternative-lengthening-of-telomeres activity. Nat. Biotechnol. *27*, 1181–1185.
11. Min, J., Wright, W.E., and Shay, J.W. (2017). Alternative Lengthening of Telomeres Mediated by Mitotic DNA Synthesis Engages Break-Induced Replication Processes. Mol. Cell Biol. *37*, e00226-17.
12. Grobelny, J.V., Godwin, A.K., and Broccoli, D. (2000). ALT-associated PML bodies are present in viable cells and are enriched in cells in the G_2/M phase of the cell cycle. J. Cell Sci. *113*, 4577–4585.
13. Zhang, J.M., Yadav, T., Ouyang, J., Lan, L., and Zou, L. (2019). Alternative Lengthening of Telomeres through Two Distinct Break-Induced Replication Pathways. Cell Rep. *26*, 955–968.e3.
14. Lu, R., Allen, J.A.M., Galaviz, P., and Pickett, H.A. (2022). A DNA-fiber protocol for single molecule analysis of telomere (SMAT) length and extension events in cancer cells. STAR Protoc. *3*, 101212.
15. Lu, R., O'Rourke, J.J., Sobinoff, A.P., Allen, J.A.M., Nelson, C.B., Tomlinson, C.G., Lee, M., Reddel, R.R., Deans, A.J., and Pickett, H.A. (2019). The FANCM-BLM-TOP3A-RMI complex suppresses alternative lengthening of telomeres (ALT). Nat. Commun. *10*, 2252.
16. Silva, B., Pentz, R., Figueira, A.M., Arora, R., Lee, Y.W., Hodson, C., Wischnewski, H., Deans, A.J., and Azzalin, C.M. (2019). FANCM limits ALT activity by restricting telomeric replication stress induced by deregulated BLM and R-loops. Nat. Commun. *10*, 2253.
17. Lu, R., Allen, J.A.M., Galaviz, P., and Pickett, H.A. (2022). A DNA-fiber protocol for single molecule analysis of telomere (SMAT) length and extension events in cancer cells. STAR Protoc. *3*, 101212.
18. Kahl, V.F.S., Allen, J.A.M., Nelson, C.B., Sobinoff, A.P., Lee, M., Kilo, T., Vasireddy, R.S., and Pickett, H.A. (2020). Telomere Length Measurement by Molecular Combing. Front. Cell Dev. Biol. *8*, 493.
19. Doksani, Y., and de Lange, T. (2016). Telomere-Internal Double-Strand Breaks Are Repaired by Homologous Recombination and PARP1/Lig3-Dependent End-Joining. Cell Rep. *17*, 1646–1656.
20. Cho, N.W., Dilley, R.L., Lampson, M.A., and Greenberg, R.A. (2014). Interchromosomal homology searches drive directional ALT telomere movement and synapsis. Cell *159*, 108–121.
21. Min, J., Wright, W.E., and Shay, J.W. (2019). Clustered telomeres in phase-separated nuclear condensates engage mitotic DNA synthesis through BLM and RAD52. Genes Dev. *33*, 814–827.
22. Pan, X., Chen, Y., Biju, B., Ahmed, N., Kong, J., Goldenberg, M., Huang, J., Mohan, N., Klosek, S., Parsa, K., et al. (2019). FANCM suppresses DNA replication stress at ALT telomeres by disrupting TERRA R-loops. Sci. Rep. *9*, 19110.

23. Verma, P., Dilley, R.L., Zhang, T., Gyparaki, M.T., Li, Y., and Greenberg, R.A. (2019). RAD52 and SLX4 act nonepistatically to ensure telomere stability during alternative telomere lengthening. Genes Dev. *33*, 221–235.

24. Loe, T.K., Li, J.S.Z., Zhang, Y., Azeroglu, B., Boddy, M.N., and Denchi, E.L. (2020). Telomere length heterogeneity in ALT cells is maintained by PML-dependent localization of the BTR complex to telomeres. Genes Dev. *34*, 650–662.

25. MacKenzie, D., Jr., Watters, A.K., To, J.T., Young, M.W., Muratori, J., Wilkoff, M.H., Abraham, R.G., Plummer, M.M., and Zhang, D. (2021). ALT Positivity in Human Cancers: Prevalence and Clinical Insights. Cancers *13*, 2384.

26. Mazzucco, G., Huda, A., Galli, M., Piccini, D., Giannattasio, M., Pessina, F., and Doksani, Y. (2020). Telomere damage induces internal loops that generate telomeric circles. Nat. Commun. *11*, 5297.

27. Carpenter, A.E., Jones, T.R., Lamprecht, M.R., Clarke, C., Kang, I.H., Friman, O., Guertin, D.A., Chang, J.H., Lindquist, R.A., Moffat, J., et al. (2006). CellProfiler: image analysis software for identifying and quantifying cell phenotypes. Genome Biol. *7*, R100.

28. Henson, J.D., Lau, L.M., Koch, S., Martin La Rotta, N., Dagg, R.A., and Reddel, R.R. (2017). The C-Circle Assay for alternative-lengthening-of-telomeres activity. Methods *114*, 74–84.

29. Özer, Ö., Bhowmick, R., Liu, Y., and Hickson, I.D. (2018). Human cancer cells utilize mitotic DNA synthesis to resist replication stress at telomeres regardless of their telomere maintenance mechanism. Oncotarget *9*, 15836–15846.

30. Garcia-Exposito, L., Bournique, E., Bergoglio, V., Bose, A., Barroso-Gonzalez, J., Zhang, S., Roncaioli, J.L., Lee, M., Wallace, C.T., Watkins, S.C., et al. (2016). Proteomic Profiling Reveals a Specific Role for Translesion DNA Polymerase eta in the Alternative Lengthening of Telomeres. Cell Rep. *17*, 1858–1871.

STAR★METHODS

KEY RESOURCES TABLE

REAGENT or RESOURCE	SOURCE	IDENTIFIER
Antibodies		
anti-RAD51, mouse monoclonal	Abcam	Cat# ab213 RRID:AB_302856
anti-RAD52, mouse monoclonal	Santa Cruz	Cat# sc-365341 RRID:AB_10851346
anti-POLH, mouse monoclonal	Santa Cruz	Cat# sc-17770 RRID:AB_2167007
anti-POLD3, mouse monoclonal	Novus	Cat# H00010714-M01 RRID:AB_606803
anti-PML, rabbit polylconal	Santa Cruz	Cat# sc-5621 RRID:AB_2166848
anti-PML, goat polyclonal	Santa Cruz	Cat# sc-9862 RRID:AB_2166847
anti-BrdU, mouse monoclonal	BD Biosciences	Cat# 347580 RRID:AB_10015219
anti-BrdU, rat monoclonal	Abcam	ab6326 RRID:AB_305426
Normal Mouse IgG	Millipore	Cat# 12-371 RRID:AB_145840
Anti-actin, rabbit polyclonal	Sigma-Aldrich	Cat# A2066 RRID:AB_476693
Anti-vinculin, mouse monoclonal	Sigma-Aldrich	Cat# V9131 RRID:AB_477629
Anti-BLM, rabbit polyclonal	Bethyl	Cat# #A300-110A RRID:AB_2064794
Anti-Histone H3, rabbit polyclonal	Cell Signaling Technology	Cat# 9715 RRID:AB_331563
Anti-Lamin B1, rabbit polyclonal	Abcam	Cat# ab16048 RRID:AB_443298
Anti-tubulin, mouse monoclonal	Abcam	Cat# ab7291 RRID:AB_2241126
Anti-FANCM (CV5.1), mouse monoclonal	Novus	Cat# NBP2-50418 RRID:AB_2716711
anti-MUS81, mouse monoclonal	Abcam	Cat# ab14387 RRID:AB_301167
Anti-FANCM (CV5.1), mouse monoclonal	Novus	Cat# NBP2-50418 RRID:AB_2716711
Alexa Fluor Plus Secondary Antibodies (AF488, 594, 647)	Thermo Scientific	Cat# A32814, A32744, A32790, A32766
Chemicals, peptides, and recombinant proteins		
Adavosertib (MK-1775)	Selleck Chemicals	Cat# S1525 CAS: 955365-80-7

(*Continued on next page*)

Continued

REAGENT or RESOURCE	SOURCE	IDENTIFIER
DMSO	Sigma-Aldrich	Cat# D2650 CAS: 67-68-5
PerfectHyb Plus hybridization buffer	Sigma-Aldrich	Cat# H7033
Thymidine	Sigma-Aldrich	Cat# T1895 CAS: 50-89-5
MES, Free Acid, ULTROL® Grade	Merck Millipore	Cat# 475893 CAS: 4432-31-9
YOYO-1 iodide	Thermo Scientific	Cat# Y3601
RO-3306	Sigma-Aldrich	Cat# SML0569 CAS: 872573-93-8
Nocodazole	Sigma-Aldrich	Cat# SML0569 CAS: 31430-18-9
Seaplaque™ Agarose	Lonza Bioscience	Cat# 50100
Proteinase K, recombinant, PCR Grade	Roche	Cat# RPROTK-RO
Agarase (0.5 U/μL)	Thermo Scientific	Cat# EO0461
Propidium iodide	Sigma-Aldrich	Cat# P4864
DAPI ready made solution	Sigma-Aldrich	Cat# MBD0015
Phi29 polymerase	NEB	Cat# M0212
T4 PNK	NEB	Cat# M0201
ATP, [γ-^{32}P]- 3000Ci/mmol 10mCi/ml EasyTide Lead, 250 μCi	PerkinElmer	Cat# NEG502A250UC
Lipofectamine RNAiMAX Reagent	Thermo Scientific	Cat# 13778075
ECL substrate	Thermo Scientific	Cat# 34580 & 34094
Protease inhibitors (Complete Mini EDTA-free cocktail tablets)	Roche	Cat# 04693124001
RNase A, DNase-free	Roche	Cat# 11119915001
Prolong Gold mounting reagent	Thermo Scientific	Cat# P36930
DMEM, high-glucose	Thermo Scientific	Cat# 11965092
Critical commercial assays		
Click-iT™ Plus EdU Cell Proliferation Kit for Imaging, Alexa Fluor™ 647 dye	Thermo Scientific	Cat# C10640
Qubit dsDNA quantitation kit	Thermo Scientific	Cat# Q32850
Protein G sepharose beads	Thermo Scientific	Cat# P3296-1ML
Nick translation kit	Roche	Cat# 10976776001
Experimental models: Cell lines		
H.sapiens: U2OS	ATCC	RRID:CVCL_0042
H.sapiens: HeLa LT	long-telomere sublcone of Parent: CVCL_0030 (O'Sullivan et al., 2014)	N/A
H.sapiens: GM847 (GM00847)	ATCC	RRID:CVCL_7908
Oligonucleotides		
Scrambled Negative siRNA Control #2	Silencer Select (Ambion)	Cat: 4390847
siPOLD3	Silencer Select (Ambion)	Cat: 4390824 siRNA ID: #s21045
siBLM	Silencer Select (Ambion)	Cat: 4390824 siRNA ID: #s1998

(*Continued on next page*)

Continued

REAGENT or RESOURCE	SOURCE	IDENTIFIER
siRAD51	Silencer Select (Ambion)	Cat: 4392422 siRNA ID: #s11735
siRAD52	Silencer Select (Ambion)	Cat: 4392422 siRNA ID: #s11747
siPML	Silencer Select (Ambion)	Cat: 4390825 siRNA ID: #s10715
siPOLH	Silencer Select (Ambion)	Cat: AM51333 siRNA ID: #s119732
siMUS81	Silencer Select (Ambion)	Cat: 4392420 siRNA ID: #s37039
siSLX4	Silencer Select (Ambion)	Cat: 4392421 siRNA ID: #s39053
siGEN1	Silencer Select (Ambion)	Cat: 4392420 siRNA ID: #s226363
PNA FISH probe TelC-TAMRA	Panagene	Cat# F2001
SLX4 (NM_032444.3) Forward primer 5′ CTTTACGCCCACAAGTTCGT 3′	Sigma-Aldrich	N/A
SLX4 (NM_032444.3) Reverse primer 5′ CACTCACGCCAAACCTGTG 3′	Sigma-Aldrich	N/A
GEN1 (NM_182625.4) Forward primer 5′ ATTGCTGGTACTTTTGACCC 3′	Sigma-Aldrich	N/A
GEN1 (NM_182625.4) Reverse primer 5′ GCATAATGTTCAGGCTTTTCCC 3′	Sigma-Aldrich	N/A
GAPDH (NM_001289745.3) Forward primer 5′ ACCCACTCCTCCACCTTTG 3′	Sigma-Aldrich	N/A
GAPDH (NM_001289745.3) Reverse prime 5′ CTCTTGTGCTCTTGCTGGG 3′	Sigma-Aldrich	N/A
Recombinant DNA		
pWZL-H2B-GFP-Hygro	was a gift from Tony Cesare, Children's Medical Research Institute	N/A
pLPC-mCherry-TRF1-Puro	was a gift from Tony Cesare, Children's Medical Research Institute	N/A
Alu repeat plasmid	pUC8 Plasmid from DeLange lab (D. Loayza).	Perlino E. et al. (1985) NAR13: 8359 PDF:6808
Software and algorithms		
Cellprofiler v2.1.1	Carpenter er al.[28]. PMID: 17076895	http://cellprofiler.org RRID:SCR_007358
Other		
PolyLysine slides	Thermo Scientific	Cat# J2800AMNZ
Nunc® Lab-Tek® II Chamber Slide™ system	Sigma-Aldrich/Thermo Scientific	Cat# 154534
FiberComb® (Molecular Combing System)	Genomic Vision	Cat# MCS-001
CombiCoverslips™	Genomic Vision	Cat# COV-002-RUO
Nanodrop1000	Thermo Scientific	Cat# ND-1000 RRID:SCR_016517
Shandon Cytospin® 4 Cytocentrifuge	Thermo Scientific	Cat# A78300002
LSM 880 Airyscan	Zeiss	RRID:SCR_020925
Biodyne B membrane	Cytiva (formerly Pall)	Cat# 60207

RESOURCE AVAILABILITY

Lead contact

Further information and requests for resources and reagents should be directed and will be fulfilled by the lead contact, Hilda A. Pickett (hpickett@cmri.org.au).

Materials availability

This study did not generate new unique reagents. Plasmids and cell lines generated in this paper are available from the lead contact upon request.

Data and code availability

- All data related to the findings of this study are available within the article, Supplementary Figures and SI files, are available from the corresponding author upon request.
- This paper does not report original code.
- Any additional information required to reanalyze the data reported in this paper is available from the lead contact upon request.

EXPERIMENTAL MODEL AND SUBJECT DETAILS

Cell culture

U-2 OS, HeLa LT and GM847 cell lines were cultured in Dulbecco's modified Eagle's medium (DMEM) (Thermo Scientific) supplemented with 10% fetal bovine serum (FBS) (Sigma) in a humidified incubator at 37°C with 10% CO_2. Cell lines were authenticated by 16-locus short-tandem-repeat profiling and routinely tested for mycoplasma contamination by CellBank Australia (Children's Medical Research Institute).

METHOD DETAILS

Synchronization of cell lines and BrdU/EdU labeling

Detailed schematics outlining all synchronization experiments are provided throughout the manuscript. For all synchronization experiments, cells were initially arrested via double-thymidine block at the G1/S boundary. Thymidine block was performed with 2 mM thymidine (Sigma) incubation for 16–24 h overnight. Cells were then synchronized in G2/M (10 h post-thymidine release), G2 arrest via addition of 10 μM RO-3306 (RO) (Sigma), G2 arrest then released into mitosis or arrested only in mitosis via nocodazole (NOC) (Sigma). Cells were synchronized in G2/M, by waiting 10 h post-thymidine release without addition of RO. Cells were arrested in G2-phase, via addition of RO at 5 h post-thymidine release, for increasing durations in the presence of RO (e.g., G2+0 h up to G2+10 h). Cells were released into mitosis from G2 arrest after washout and replacement with fresh media for up to 40 min or up to 2 h with NOC to trap cells in mitosis. Cells were directly arrested in mitosis via release from thymidine with NOC for 15 or 25 h post-thymidine release.

For FANCM, PML, BLM, POLD3, RAD51 and RAD52 siRNA treatments in combination with cell synchronization, siRNA transfections were performed after release from the first thymidine block, but before the second thymidine block, to overcome downstream cell cycle effects of the siRNA intervention confounding synchronization at the G1/S boundary. For MUS81, SLX4 and GEN1 siRNA depletions, asynchronous cells were transfected for 24 h, subjected to a single thymidine block for 16–24 h then released and analyzed in G2 or M as previously described (Methods S5B).

100 μM BrdU and 10 μM EdU concentrations were used for labeling of synthesis in cells. Labeling with either BrdU or EdU, for all microscopy experiments, was performed for the last hour in G2 (prior to indicated G2 arrest timepoint) or for 40 min for the duration of mitotic release from G2 (in the absence of NOC). This is consistent with the synchronization methods used by several publications examining telomere MIDAS.[11,29,30] For single-molecule analysis of telomeres (SMAT) and newly synthesized telomere/C-circle analysis, G2 labeling was performed for the last 2 h prior to indicated G2 arrest timepoint or for 2 h for the duration of G2 release into mitosis in the presence of NOC.

For experiments examining the retention of EdU+ telomeres in the subsequent G1-phase, G2-arrested cells were released into the subsequent G1-phase, after EdU labeling during G2 arrest. This was achieved by washing G2 arrested cells and replacing with fresh media supplemented with thymidine for 9–11 h. We also examined the retention of SMAT EdU+ telomere extension events into the subsequent G1 after labeling for 2 h during mitotic release from G2. Specifically, we selected mitotic cells after labeling, via mitotic-shake-off. Cells were then spun down, washed twice with PBS, then reseeded in fresh media and resynchronized in G1 with thymidine for 9–11 h.

Genetic constructs and plasmids

For live-cell fluorescence monitoring of telomeres and chromatin, U-2 OS cells, were stably transduced with pWZL-H2B-GFP and pLPC-mCherry-TRF1 via 2nd generation lentiviral packaging system. Transduced cells were maintained in puromycin and neomycin selection during passage.

RNA interference

Transient protein depletion was performed with the following Silencer Select siRNAs, designed and synthesized by Invitrogen (Ambion): POLD3 #s21045, BLM #s1998, RAD51 #s11735, RAD52 #s11747, MUS81 #s37039, SLX4 #s39053 GEN1 #s226363, POLH (pol η) #s119732, PML #s10715 and Silencer Select RNAi siRNA Negative Control #2 (#4390847). Cells were either forward or reverse transfected at 20–50% confluency with Lipofectamine RNAiMAX (Life Technologies) at a final siRNA concentration of 30 nM. Knockdown was confirmed by Western blot analysis or qRT-PCR (see key resources table for list of qRT-PCR primers).

Genomic DNA extraction and purification

Cells were harvested by trypsinization and lysed in DNA extraction buffer (100 mM Tris-HCl pH 7.6, 100 mM NaCl, 10 mM EDTA, 1% w/v N-lauroylsarcosine). Lysates were digested with 50 μg/mL RNase A for 20 min at room temperature, followed by digestion with 100 μg/mL proteinase K overnight at 55°C. DNA was extracted using two rounds of phenol/chloroform/isoamyl alcohol (25:24:1) solution (Sigma Aldrich) in MaXtract High Density tubes (Qiagen). DNA was precipitated with 0.1 volumes of 3 M sodium acetate pH 5.2 and 2.5 volumes of cold 100% ethanol. DNA was washed with 70% ethanol, dried, and dissolved in 10 mM Tris-HCl pH 7.6 (if further enzymatic reactions were performed) or 10 mM TE buffer.

Immunoblotting

Cells were collected and lysed in RIPA buffer (50 mM Tris-HCl pH 7.6, 150 mM NaCl, 1% Nonidet P-40, 0.5% sodium deoxycholate, 0.1% SDS) supplemented with Complete protease inhibitor cocktail (Roche). Protein concentration was quantitated via the BCA assay (Thermo Scientific) and lysates resolved on either 3–8% Tris-Acetate or 4–12% Bis-Tris gels (Invitrogen). Proteins were transferred to Immobilon P PVDF membranes (Millipore). Membranes were optionally stained with Ponceau S (Sigma) and blocked with either 5% non-fat dried milk powder (NFDM) or bovine serum albumin (BSA) in PBST. Blots were incubated with primary antibody (for list of antibodies, see key resources table) at either 4°C overnight or room temperature for 2 h. Membranes were then washed with PBST and incubated with corresponding HRP-conjugated secondary antibodies (Dako) for 1 h at room temperature. Protein bands were visualized using either PICO PLUS or FEMTO enhanced chemiluminescence reagents (Thermo Scientific). Uncropped blots are available in Data S3.

Single molecule analysis of telomeres (SMAT)

DNA fibers, stained for telomeres, DNA, and labeled for EdU, were prepared as described previously for U-2 OS, HeLa LT and GM847 cells.[17] SMAT was performed on EdU-labelled G2 arrested cells and mitotic cells (selected via mitotic shake-off) released for 2 h from G2 arrest and cells labeled for 2 h during G2/M defined as 9–11 h post-thymidine release. G2 arrested cells were labeled for the last 2 h prior to the indicated timepoint. Mitotic cells were labeled either for 2 h after G2 release in the presence of NOC or in M arrested cells (NOC already present). 40 nM nocodazole was also added to arrest cells in mitosis. Mitotic cells were selected via mitotic shake-off and released into G1 with fresh media. Cells were allowed to recover for 4 h then pulsed with EdU for 2 h prior to harvesting. Scoring of telomere extension events and non-terminal EdU tracts was performed as described[17] for at least 450 telomeres across three experiments.

Standard C-circle assay and newly synthesized C-circle assay (native BrdU immunoprecipitation)

C-circles were amplified with Phi29 polymerase (NEB) using dATP, dTTP and dGTP nucleotide mix (NEB) as previously described.[10,28] C-circle products were dot blotted onto Biodyne B membranes (Pall) and pre-hybridized in PerfectHyb Plus (Sigma) for at least 30 min. Radiolabeled telomeric C-probe was then added and blots were hybridized overnight at 37°C as previously described.[10] Blots were washed with 0.5× SSC, 0.1% SDS three times for 5 min each then exposed to phosphor screen. Imaging was performed on the Typhoon FLA 7000 system (GE Healthcare) with a PMT of 750 V.

For newly synthesized C-circle analysis, cells were labeled for 2 h with 100 μM BrdU. gDNA was extracted and digested with HinfI and RsaI and subject to BrdU immunoprecipitation, as previously described, but without heat or alkaline denaturation.[15] In brief, 6 μg input of genomic DNA was incubated per 60 μL of Protein G agarose beads overnight at 4°C. Immunoprecipitated DNA was then eluted in 100 μL of elution buffer (50 mM $NaHCO_3$ and 1% v/v SDS), purified with a QIAquick PCR Purification Kit (Qiagen), and redissolved in 25 μL TE. C-circle amplification and detection was carried out as described previously.[10]

Cell fractionation for Southern blotting

Harvested cells were placed on ice prior to processing. 1 mM PMSF and 1× protease inhibitor cocktail were supplemented for all lysis buffers when extracting protein but omitted when isolating DNA. Cells were lysed in 200 μL of E1 buffer (50 mM HEPES-KOH pH 7.5, 140 mM NaCl, 1 mM EDTA, 10% glycerol, 0.5% NP-40, 0.25% Triton X-100), mixed and centrifuged for 2000 g for 2 min. After setting aside the supernatant corresponding to cytoplasmic fraction, the pellet was washed a further two times with E1 buffer at 1,100 g for 2 min (this speed used for all subsequent washes) then incubated for 10 min on ice on the second wash. The pellet was then suspended in 30 μL of E2 buffer (10 mM Tris pH, 200 mM NaCl, 1 mM EDTA, 0.5 mM EGTA pH 8), incubated on ice for 10 min and supernatant corresponding to nucleoplasmic fraction collected. The pellet was further washed twice with E2 buffer and incubated on ice for the second wash for 10 min. The final chromatin fraction was isolated by suspending the pellet in 50 μL of E3 buffer (500 mM Tris pH 6.8, 500 mM NaCl). For mitotic cells, the nucleoplasmic and cytoplasmic fractions were pooled. Fractions were then adjusted to a final concentration of 1% NLS and with DNA Extraction Buffer up to 200 μL

and subject to DNA isolation as described earlier. For Southern blotting analysis, the DNA content of the chromatin fraction was quantitated via Nanodrop. At least 4 μg of chromatin DNA were isolated per sample. The proportion of cytoplasmic or nucleoplasmic fraction corresponding to 400 ng of chromatin DNA input volume was used for Southern blotting. For Western blot validation of cell fractionation, isolated fractions were diluted in LDS buffer (using 4X LDS (without bromophenol blue) and 10× reducing agent (Invitrogen)). Protein concentration was quantitated via BCA assay (ThermoFisher) then LDS lysates diluted 1:100 with 10 mg/mL bromophenol blue (Sigma) prior to polyacrylamide gel electrophoresis (PAGE).

Immunofluorescence (IF) and fluorescence in situ hybridization (FISH)

IF and telomere FISH were performed on both interphase nuclei and mitotic cells. For interphase experiments, cells were grown on coverslips or LabTek chamber slides (Thermo Scientific). Mitotic cells were harvested by mitotic shake-off, then cytospun onto Polylysine slides (ThermoFisher) at 800 rpm for 10 min using funnels on the Shandon Cytospin 4 (ThermoFisher). Both interphase and mitotic cells were fixed with ice-cold 4% formaldehyde PBS solution for 10 min, washed twice with PBST and PBS then permeabilized with 0.5% KCM buffer (120 mM KCl, 20 mM NaCl, 10 mM Tris pH 7.5, 0.5% Triton). Coverslips were blocked with antibody-dilution buffer (20 mM Tris–HCl, pH 7.5, 2% w/v BSA, 0.2% v/v fish gelatin, 150 mM NaCl, 0.1% v/v Triton X-100 and 0.1% w/v sodium azide) and 0.1 mg/mL RNaseA for 1 h at RT. Cells were incubated with primary antibodies for 2 h at room temperature or 4°C overnight, then incubated with 1:1,000 dilution of appropriate Alexa Fluor conjugated secondary antibodies (Thermo Scientific). Coverslips were then rinsed with PBS and fixed with 4% v/v formaldehyde at room temperature prior to telomere FISH. Coverslips were subjected to a graded ethanol series (75% for 2 min, 85% for 2 min, and 100% for 2 min) and allowed to air-dry. Dehydrated coverslips were overlaid with 0.3 μg/ml FAM–OO-$(CCCTAA)_3$ telomeric PNA probe (Panagene) in PNA hybridization solution (70% deionized formamide, 0.25% v/v NEN blocking reagent (PerkinElmer), 10 mM Tris–HCl, pH 7.5, 4 mM Na_2HPO_4, 0.5 mM citric acid, and 1.25 mM $MgCl_2$), denatured at 80°C for 5 min, and hybridized at room temperature overnight. Coverslips were washed twice with PNA wash A (70% formamide, 10 mM Tris pH 7.5) and then PNA wash B (50 mM Tris pH 7.5, 150 mM NaCl, 0.8% Tween-20) for 5 min each. 2 μg/mL DAPI was added to the second PNA wash B. Finally, coverslips were rinsed briefly in deionized water, air dried and mounted with Prolong Gold mounting medium (Thermo Scientific). Microscopy images were acquired on a Zeiss Axio Imager.Z2 microscope with Plan-APO 63x/1.4-Oil (25°C) objective with appropriate filter sets. For QIBC, the Plan-Neofluar 40x/1.3-Oil (25°C) objective was used.

Dropped chromosome metaphase spread analysis

Metaphase chromosome spreads were performed as previously described with modifications (Sobinoff, 2017). Mitotic cells were obtained from mitotic release or arrest via mitotic shake-off then swelled with 0.1% w/v sodium citrate-dihydrate, 0.1% w/v KCl hypotonic solution. Cell suspensions (in PBS) were diluted 1:10 with 3:1 ratio methanol:acetic acid then fixed with three washes of methanol:acetic acid. Cells were then dropped onto microscope slides over a 75°C water bath and left to dry/cure at least overnight. Slides were then treated with 100 μg/ml DNase-free RNase A (Sigma) in 2× SSC for 30 min at 37°C, rinsed in PBS, and post-fixed in 4% formaldehyde for 10 min. Labelling of EdU was subsequently performed prior to fluorescence *in-situ* hybridization (FISH). Slides were then probed with telomere C-probe (0.3 μg/mL Alexa 488-OO-$(CCCTAA)_3$), denatured at 80°C for 2 min, and hybridized overnight at room temperature. Slides were washed for 15 min with PNA wash A then again with PNA wash B, and stained with DAPI in PBS for 5 min. Slides were then air-dried and mounted with Prolong Gold antifade solution.

BrdU and EdU detection for microscopy

EdU labeled cells were detected with the Click-iT Plus Alexa Fluor 647 kit (Thermo Scientific) according to the manufacturer's instructions. Click-labelling was performed before blocking with ABDIL and RNaseA. For SMAT analysis, conjugation of incorporated EdU was performed concomitant with YOYO-1 staining of DNA fibers, as previously described.[17] BrdU-labelling was detected via antibody and was performed as described earlier.

Live cell imaging

pWZL-H2B-GFP and pLPC-mCherry-TRF1 transduced U-2 OS cells were observed on the LSM880 Airyscan (Zeiss) using the confocal mode. Scans were performed across a 350 × 350 (0.39 × 0.39 × 1 μm scaling) linear scanning window with a Plan-APO 63×/1.4-Oil (37°C) objective. The focal plane was defined by manual focus of the base of mitotic cells and drift compensated by Definite Focus. 15 z-stacks (above the focal plane) with 14 μm separation were acquired every 10 s with the 561 nm DPSS laser at 4% power.

Cellprofiler microscopy image analysis

Z-stacks from ZEN microscopy files (.czi) were processed into maximum projections using ZEN desk 2011 software (Zeiss) and imported into Cellprofiler v2.1.1[27] for analysis. The DAPI channel was used to mask individual nuclei as primary objects. Foci within each segmented nucleus were identified using an intensity-threshold based mask. Colocalization between two foci was defined by setting 20% as the minimum overlapping area of first object overlapping the second object.

For QIBC analysis, in addition to the previously described method of colocalization scoring using Cellprofiler, DAPI nuclear intensity was used to determine cell cycle stage and EdU nuclear intensity was used to identify S-phase.

Automated ECTR analysis of cytocentrifuged mitotic cells was performed via addition of a cytoplasmic mask extending beyond the chromosome (DAPI) mask, arbitrarily defined as a 90 pixel distance based on background cytoplasmic PML staining. In the event that metaphases were close enough to cause overlapping cytoplasmic masks, Cellprofiler splits contacting cytoplasmic masks between two cells at the halfway point between the two nuclei. For representative Cellprofiler pipeline analysis images, see Methods S4. The Cellprofiler pipeline used for analysis can be downloaded from File S1.

Flow cytometry

Ethanol-fixed single-cell suspensions were stained for DNA analysis with 2 mg/mL RNase A and 0.1 mg/mL propidium iodide (PI) in 0.25 mL PBS. Cells were incubated for 30 min at 37°C then equilibrated at room temperature in the dark for at least 10 min. Cells were analyzed by BD FACSCanto II Flow Cytometry (BD Biosciences) using an air-cooled 488 nm argon laser to excite PI. A total of 9,000–10,000 stopping gate events were collected at an approximate flow rate of 200 events/s. The forward scatter (FSC, size) and side scatter (SSC, internal granularity) of each cell were recorded. To discriminate and eliminate cell debris and doublets, the pulse area (PI-A) was plotted against the pulse width (PI-W). Doublets identified as cells with greater than 2N DNA content were eliminated. Cell cycle population analysis was conducted with FlowJo v7 software (FlowJo).

QUANTIFICATION AND STATISTICAL ANALYSIS

All statistical analysis was performed using Graphpad Prism 9. Details regarding quantitation and statistical analysis are provided in the figures and figure legends. Two-sided Student's *t* test was performed on data assumed to be normally distributed, while the two-sided Mann-Whitney test was performed on data assumed to be non-normally distributed. When multiple comparisons, involving more than 4, were made between treatments, one way ANOVA with the appropriate Brown-Forsythe and Welch ANOVA or Dunnett's ANOVA test was performed for normally distributed data. For non-normally distributed data involving multiple comparisons, the Kruskal-Wallis ANOVA test was performed. For p values that were above 0.05 but less than 0.1, the exact values are indicated in figures.